JOURNAL OF NANOMATERIALS AND DEVICES
Jul-Dec 2023, VOL. 1, ISSUE 1, pp. 42-48
https://doi.org/10.61577/jnd.2023.100008

RESEAPRO JOURNALS

OPEN ACCESS

ORIGINAL ARTICLE

Synthesis of nanocrystalline ZnS thin films by chemical bath deposition: Influence of hydrazine hydrate concentration

Vikram P. Bhalekar[1]*, Shivaji M. Sonawane[2], Nilesh S. Kanhe[3], Ashok B. Nawale[4]

[1]Department of Physics, Arts, Science and Commerce College, Rahata, Ahilyanagar
[2]Department of Physics, Bharatiya Jain Sanghatana's A. S. and C College, Wagholi, Pune
[3] Department of Physics, Arts, Commerce and Science College, Satral, Ahilyanagar
[4] Department of Physics, Govt. Vidarbha Institute of Science and Humanities, Amravati

ABSTRACT

Nanocrystalline Zinc Sulphide (ZnS) thin films were deposited via Chemical Bath Deposition (CBD) method using varying concentrations of Hydrazine Hydrate (H.H., 0-2.0 M) as a complexing agent. The earlier studies have typically examined only selected properties, limited concentration ranges, or a single thermal state (as deposited or annealed), in comparison, the present work provides the effects of H.H. concentration and post-deposition annealing on structural, optical, photoluminescence, morphological and compositional properties were systematically investigated. X-ray Diffraction (XRD) of the precipitated powder confirmed the formation of cubic-phase ZnS with average crystallite sizes of 4-5 nm. The optical absorption measurements showed that the direct band gap of as-deposited films increased with H.H. concentration, consistent with a decrease in particle size due to enhanced nucleation. Annealing reduced the band gap owing to particle growth and coalescence. Photoluminescence spectra (excitation at 345 nm) exhibited band-edge emission near 358-360 nm together with defect-related emissions associated with sulfur and zinc vacancies. Scanning Electron Microscopy (SEM) revealed that H.H. improves film uniformity, compactness and reduces particle size, while annealing produces more compact granular morphology. Energy Dispersive X-Ray Analysis (EDAX) showed that the concentration of H.H. and annealing have a strong influence on the atomic ratio of Zn and S. The result show that the concentration of hydrazine hydrate is good parameter to adjust the nanocrystalline properties of ZnS thin films with direct relevance to Cd-free buffer layers for optoelectronic applications.

KEY WORDS

ZnS; Nanocrystals; Chemical bath deposition; Hydrazine hydrate; Optical band gap; Photoluminescence; SEM; XRD; Quantum confinement

ARTICLE HISTORY

Received 13 September 2023;
Revised 06 December 2023;
Accepted 8 December 2023

Introduction

Zinc sulfide is a wide-band-gap II-VI semiconductor with bulk band-gap energies of approximately 3.54 eV (cubic/sphalerite) and 3.91 eV (hexagonal/wurtzite) at room temperature [1-4]. Its high refractive index, excellent visible-region transmittance, and good chemical stability render it attractive for electroluminescent devices, flat-panel displays, sensors, photocatalysis, and especially as a cadmium-free buffer layer in thin-film solar cells based on Copper Indium Gallium Selenide (CIGS) Cu (In,Ga)Se_2 and Copper Zinc Tin Sulfide (CZTS) $Cu_2ZnSn(S,Se)_4$ [5-8]. When the crystallite size approaches the exciton Bohr radius of ZnS (approximately 2.5 nm), quantum confinement effects become pronounced, enabling size-tunable optical and electronic properties that are highly desirable for device engineering. When the crystallite size approaches the exciton Bohr radius, quantum confinement effects become pronounced, enabling size-tunable optical and electronic properties [9,10]. ZnS thin films have been synthesized by different physical and chemical techniques such as electrodeposition, sol-gel, magnetron sputtering, atomic layer deposition, chemical vapor deposition, spray pyrolysis, Successive Ionic Layer Adsorption and Reaction (SILAR), sputtering, pulsed laser deposition, CBD, etc. [11-27]. Most of these methods require vacuum systems, sophisticated instrumentation, or elevated temperatures, which increase cost and limit substrate choice [28]. Among deposition techniques, CBD is particularly advantageous because it is simple, low-cost, requires only mild temperatures (typically 60-90°C), and is suitable for large-area, conformal coatings on temperature-sensitive substrates [29,30]. In a typical CBD process of ZnS, zinc salts (sulfate, chloride, or acetate), thiourea as the sulfur source, and one or more complexing agents are employed in aqueous alkaline media. Hydrazine hydrate ($N_2H_4{\cdot}H_2O$) is widely used as a complementary complexing agent. It stabilizes Zn^{2+} ions, modulates the release of free metal ions, accelerates the deposition rate, improves film adhesion and uniformity, and suppresses homogeneous precipitation in the bulk solution. These functions arise from the dual complexing and mild reducing character of hydrazine [31,32].

Despite extensive prior work, a comprehensive understanding of how H.H. concentration simultaneously governs nucleation density, quantum-confinement effects, defect-related luminescence, morphology, and Zn/S stoichiometry remains incomplete. Most previous investigations examined only selected properties (optical or morphological), restricted concentration ranges, or a single thermal state. The present study systematically varies H.H. concentration from 0 to 2.0 M and evaluates the resulting changes in both as-deposited and annealed nanocrystalline

***Correspondence:** Vikram P. Bhalekar, Department of Physics, Arts, Science and Commerce College, Rahata, India, email: bhalekarvp@gmail.com

ZnS films on identical sample sets. The work demonstrates that H.H. concentration is a powerful, independent parameter for engineering multiple functional properties relevant to optoelectronic and photovoltaic applications.

Several recent studies have examined the influence of complexing agents, including H.H., on CBD-ZnS films [33-43]. The reported optical changes with complexing-agent concentration, and other works have focused on pH or ammonia-free routes [33,36,37,43]. Early kinetic studies established that the deposition proceeds via the slow release of S^{2-} from thiourea and the controlled dissociation of zinc ammine or zinc hydrazine complexes. Doña and Herrero provided detailed process and film characterization of CBD-ZnS, highlighting the importance of bath chemistry. Subsequent work by Oladeji and Chow explored multilayer CdS/ZnS structures, while Goudarzi et al. demonstrated ammonia-free routes that still relied on alternative complexants. More recent investigations have focused specifically on hydrazine [34]. Kim et al. reported that hydrazine catalytically enhances the growth rate of ZnS films intended for CIGS buffer layers and improves film quality [16]. Lee and Kim examined the effect of hydrazine as a complexing agent on growth kinetics and film morphology [35]. Arsad et al. published a comprehensive review of CBD variables (pH, temperature, complexant concentration, substrate) and their influence on ZnS film properties, underscoring the sensitivity of optical and structural characteristics to bath composition [43]. Other studies have varied pH, employed alternative complexing agent such as tri-sodium citrate, or compared CdS and ZnS films prepared under similar conditions [36,37,39,40].

Optical band-gap shifts, morphology improvements, and stoichiometry changes have been reported, yet few works present comparison of as-deposited versus annealed films across structural, optical, photoluminescence, morphological, and compositional domains for a systematic series of H.H. concentrations. Consequently, the quantitative relationship between H.H. concentration, nucleation density, quantum confinement, defect luminescence, and Zn/S ratio has not been fully mapped. The present investigation fills this gap by providing a unified data set and placing the observations in the context of the existing literature.

Experimental

Glass substrates (1 × 3 cm^2) were cleaned sequentially with detergent solution, deionized water, acetone and dilute HCl (1:10), followed by extensive rinsing with deionized water and drying in an oven at 60 °C. The chemical bath consisted of an aqueous solution of zinc sulfate heptahydrate ($ZnSO_4{\cdot}7H_2O$, Sigma-Aldrich, ≥ 99 % purity) at 0.2 M, thiourea ($SC(NH_2)_2$, Merck, ≥ 99 % purity) at 0.4 M, ammonia (25 % aqueous solution, Thermo Fisher Scientific, analytical grade) adjusted to pH 10.5 ± 0.2, and hydrazine hydrate ($N_2H_4{\cdot}H_2O$, Sigma-Aldrich, 80 % purity) at concentrations of 0, 0.5, 1.0, 1.5, and 2.0 M. The total bath volume was 100 mL. The zinc precursor employed throughout this study was zinc sulfate. The bath temperature was maintained at 75 ± 2°C with continuous magnetic stirring at 300 rpm. Substrates were immersed vertically for a fixed deposition time of 90 min. After deposition, films were rinsed thoroughly with deionized water and dried in air at room temperature. Selected films were annealed in air at 300°C for 1 h to examine the influence of thermal treatment.

To assess reproducibility, three independent deposition runs were performed for each H.H. concentration; optical band-gap values remained consistent within ± 0.05 eV and morphological features were visually reproducible. Precipitate formed in the bath during deposition was collected by centrifugation, washed, and dried for powder XRD analysis.

Structural characterization was performed using a Rigaku Miniflex X-ray diffractometer (Japan) with Cu-Kα radiation (λ = 1.5406 Å) over the 2θ range 20-80°. Optical absorption spectra were recorded with a Shimadzu UV-2600 UV-Vis spectrophotometer (Japan) in the 200-1100 nm range. Photoluminescence (PL) measurements were carried out on a Horiba FluoroMax-4 spectrofluorometer (Japan/USA) with an excitation wavelength of 345 nm. Surface morphology was examined by a JEOL JSM-IT300 scanning electron microscope (Japan), and elemental composition together with EDAX spectra were obtained using the same instrument equipped with an Oxford Instruments energy-dispersive X-ray spectrometer (United Kingdom).

Results and Discussion

Structural analysis

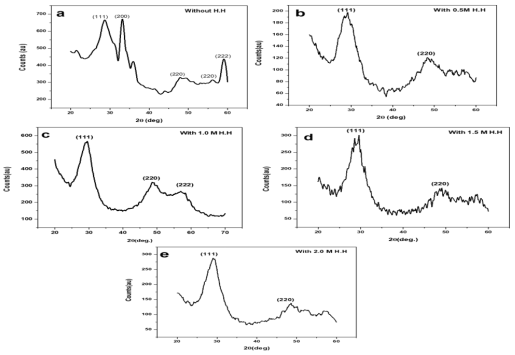

Figure 1. X-ray diffraction patterns of ZnS powder precipitated at hydrazine hydrate concentrations of (a) 0 M and with increasing (b) 0.5 M, (c) 1 M, (d) 1.5 M, (e) 2 M. Peaks are indexed to the cubic (zinc-blende) phase.

As-deposited ZnS thin films were too thin to yield clear XRD peaks. Consequently, the powder precipitated during film growth was analyzed. Figure 1 shows the XRD patterns of ZnS powder obtained at different H.H. concentrations. Diffraction peaks corresponding to the (111), (220), and (311) planes match the standard JCPDS data (Card No. 05-0566) for cubic ZnS, confirming the zinc-blende structure [44,45]. A weak peak near 2θ = 36° in the sample prepared without H.H. is attributed to ZnO impurity.

Average crystallite size was calculated using the Scherrer formula:

$$D = \frac{K\lambda}{\beta cos\theta}$$

Where (D) is the crystallite size, K=0.9, λ= is X-ray wavelength, θ= Bragg angle and β = full width at halfmaximum (FWHM) in radians , λ= 1.54Å , X-ray wavelength [46].

https://doi.org/10.61577/jnd.2023.100008

Table 1. The FWHM values of the principal XRD reflection and the corresponding average crystallite sizes for ZnS powder precipitated at different H.H. concentrations.

Concentration of H.H.	FWHM
0 M	2.93
0.5 M	3.62
1.0 M	3.49
1.5 M	3.14
2.0 M	3.02

Table 1 lists the FWHM values of the principal XRD reflection and the corresponding average crystallite sizes. The Scherrer-derived sizes confirm the nanocrystalline character of the precipitated ZnS (4–5 nm). The initial rise in FWHM (smaller effective size) with moderate H.H. addition reflects increased nucleation density arising from controlled release of free Zn^{2+} ions and catalytic acceleration of sulfide formation. At the highest concentrations the reaction kinetics become excessively rapid, favoring agglomeration and a modest recovery in apparent size. The weak ZnO-related feature in the H.H. free sample is consistent with incomplete suppression of hydroxide pathways in the absence of the complementary complexant. These trends align with the established dual role of hydrazine in CBD-ZnS systems [33,35,36]. Recent reports similarly note that hydrazine modulates nucleation density, supporting the observed size variation [35,43].

Optical absorption analysis

The systematic blue-shift of the absorption edge (increase in direct optical band gap) with rising H.H. concentration is a direct manifestation of quantum confinement. Higher nucleation density produces a larger population of smaller nanoparticles on the substrate, increasing the effective band gap relative to bulk cubic ZnS (~3.54 eV). This size-dependent optical tunability is a hallmark of nanocrystalline II-VI semiconductors near the exciton Bohr radius [8,47].

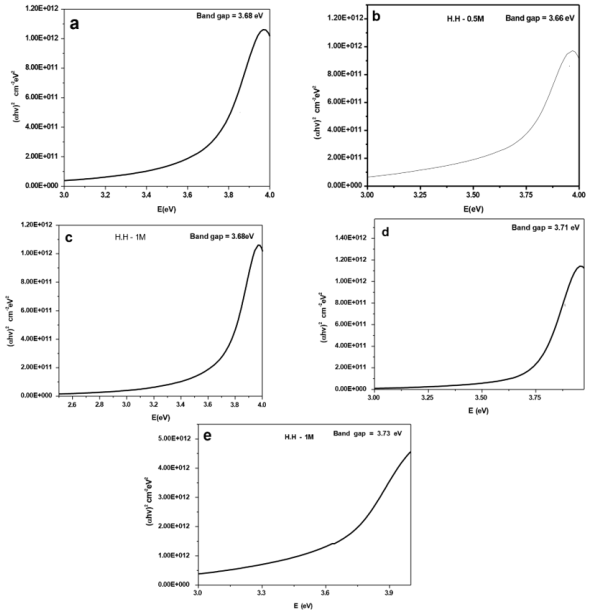

Figure 2. Optical absorption spectra of as-deposited ZnS thin films prepared at different hydrazine hydrate concentrations (a) 0 M and with increasing (b) 0.5 M, (c) 1 M, (d) 1.5 M, (e) 2 M.

Figure 2 presents the optical absorption spectra of as-deposited ZnS thin films. The systematic blue-shift of the absorption edge (increase in direct optical band gap) with rising H.H. concentration is a direct manifestation of quantum confinement. Higher nucleation density produces a larger population of smaller nanoparticles on the substrate, increasing the effective band gap relative to bulk cubic ZnS (~3.54 eV).

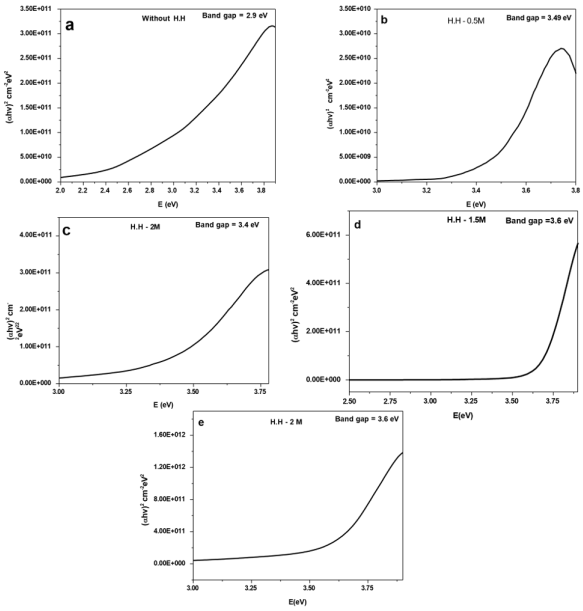

Figure 3. Optical absorption spectra of annealed ZnS thin films prepared at different hydrazine hydrate concentrations (a) 0 M and with increasing (b) 0.5 M, (c) 1 M, (d) 1.5 M, (e) 2 M.

Figure 3 shows a spectrum of annealed films; annealing produces a red-shift (decrease) of the band gap relative to the corresponding as-deposited films, attributable to grain growth and reduction of quantum confinement [13,48]. This behavior is well documented for annealed CBD-ZnS [49,50].

Photoluminescence analysis

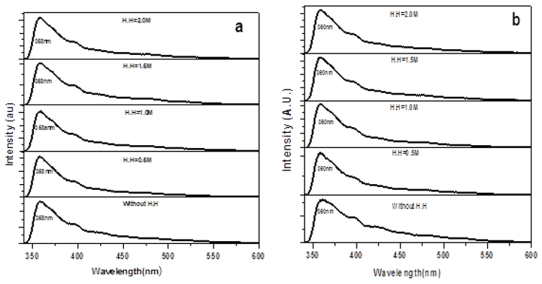

Figure 4. Room-temperature photoluminescence spectra of (a) as-deposited and (b) annealed ZnS thin films (excitation 345 nm).

Figure 4 displays the room-temperature photoluminescence spectra of (a) as-deposited and (b) annealed ZnS thin films (excitation 345 nm). The spectra exhibit a near-band-edge ultraviolet emission (~358 nm) together with defect-related blue-green bands (~425 nm and ~470 nm) assigned to sulfur vacancies (Vs) and zinc vacancies (V_{Zn}) respectively. A weaker feature near 370 nm is attributable to residual ZnO. Peak positions are essentially independent of H.H. concentration,

https://doi.org/10.61577/jnd.2023.100008

indicating that the dominant radiative centers remain the same; intensity variations reflect changes in defect density linked to particle size and stoichiometry. Upon annealing, a slight red-shift of the band-edge emission (to ~360 nm) corroborates the increase in average particle size. Defect emissions persist, showing that sulfur and zinc vacancies are not fully annealed out under the thermal conditions employed.

In figure 4, the spectra display a near-band-edge ultraviolet emission (~358 nm) together with defect-related blue-green bands (~ 425 nm and ~ 470 nm) assigned to sulfur vacancies (Vs) and zinc vacancies (V_{Zn}) respectively. A weaker feature near 370 nm is attributable to residual ZnO [51-53]. Peak positions are essentially independent of H.H. concentration, indicating that the dominant radiative centers remain the same; intensity variations reflect changes in defect density and non-radiative pathways linked to particle size and stoichiometry and figure 4 the slight red-shift of the band-edge emission (to ~360 nm) corroborates the increase in average particle size upon annealing. Defect emissions persist, showing that sulfur and zinc vacancies are not fully annealed out under the thermal conditions employed.

Morphological analysis

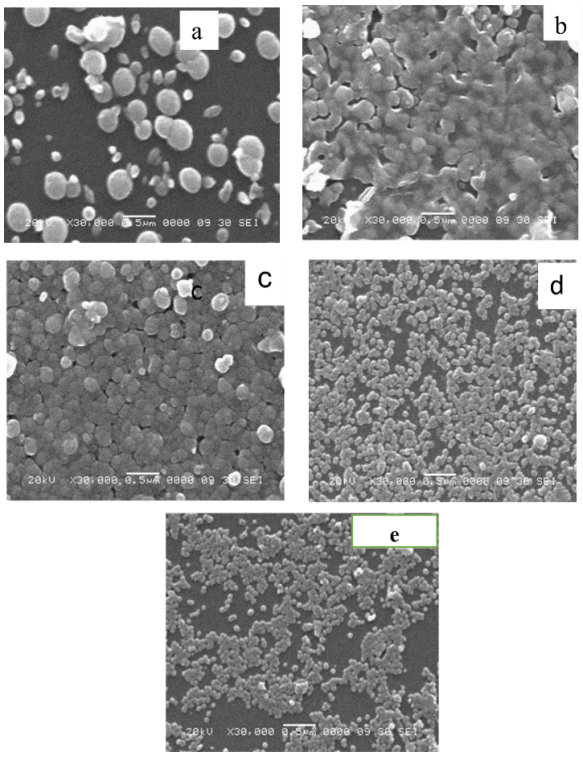

Figure 5. Scanning electron micrographs of as-deposited ZnS thin films prepared without (a) 0 M and with increasing (b) 0.5 M, (c) 1 M, (d) 1.5 M, (e) 2 M concentrations.

Figure 5 shows scanning electron micrographs of as-deposited ZnS thin films. Deposition without H.H. yields incomplete and non-uniform coverage. Addition of H.H. improves nucleation and growth, producing compact, uniform films. Particle density increases and particle size decreases with rising H.H. concentration, in agreement with the optical results. The film prepared with 1.0 M H.H. exhibits particularly favorable granular morphology.

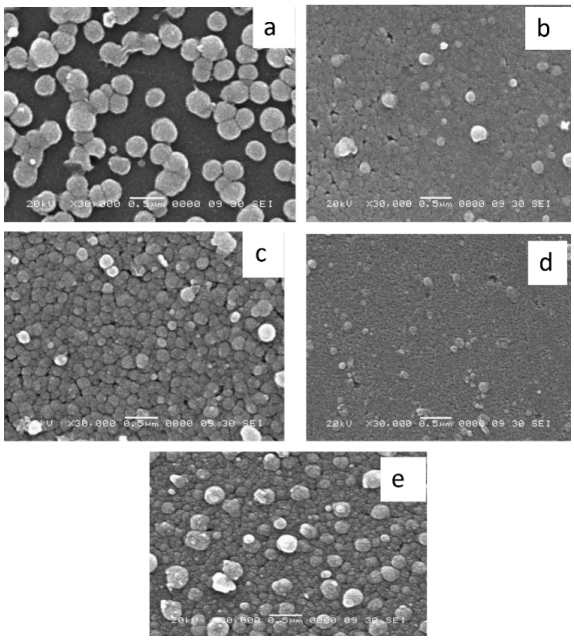

Figure 6. Scanning electron micrographs of annealed ZnS thin films prepared without (a) 0 M and with increasing (b) 0.5 M, (c) 1 M, (d) 1.5 M, (e) 2 M concentrations.

Figure 6 presents the micrographs of annealed films. Annealing produces larger grains, less distinct boundaries, and overall densification via coalescence and sintering. These morphological changes are responsible for the observed reduction in optical band gap and the modest modification of photoluminescence intensities [54-56].

Energy-dispersive X-ray analysis (EDAX)

Table 2. Atomic percentages of Zn and S obtained by EDAX for as-deposited and annealed ZnS thin films.

	As-deposited films At Wt %		Annealed Films At Wt %	
ZnS	**Zn**	**S**	**Zn**	**S**
Without H.H	58.04	41.96	47.16	52.84
With 0.5M H.H	56.35	43.65	50.93	49.07
With 1.0M H.H	54.94	45.26	54.31	45.69
With 1.5M H.H	44.82	55.18	49.87	50.13
With 2.0M H.H	44.11	55.89	55.82	44.18

Table 2 lists the atomic percentages of Zn and S, in as-deposited films the progressive decrease in Zn at. % (and corresponding rise in S) with increasing H.H. concentration is attributable to the mild reducing action of hydrazine, which partially reduces Zn^{2+} and alters the relative incorporation rates of the cations and anions [57]. After annealing the opposite trend (relative Zn enrichment / S depletion at higher original H.H. levels) is explained by preferential volatilization of sulfur during thermal treatment, a well-documented process in nanocrystalline ZnS [58]. The data demonstrate that both H.H. concentration and post-deposition annealing provide independent levers for tuning film stoichiometry, which in turn influences defect densities and optical response.

https://doi.org/10.61577/jnd.2023.100008

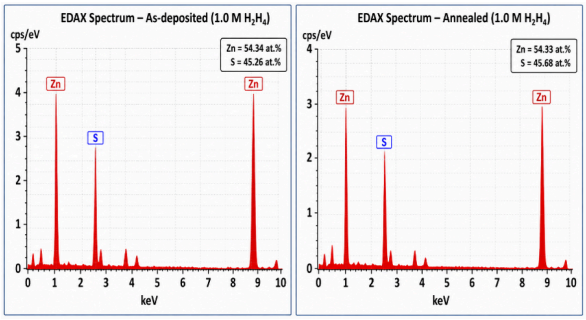

Figure 7. EDAX spectra with 1.0 M H.H of the as-deposited and annealed ZnS thin films, confirming the presence of Zn and S as the principal elements and the absence of significant impurities within the detection limit.

Figure 7 shows the illustrative EDAX spectra of the 1.0 M H.H. ZnS thin films confirm the presence of zinc and sulfur as the primary constituent elements, with characteristic peaks appearing at the expected energies (Zn L-lines near 1 keV, S K-line near 2.3 keV, and Zn K-lines near 8.6-9.6 keV). The as-deposited film is slightly zinc-rich (Zn = 54.94 at %, S = 45.26 at %), while the annealed film shows a modest shift toward improved stoichiometry (Zn = 54.31 at. %, S = 45.69 at. %). These results indicate that both the hydrazine hydrate concentration and the post-deposition annealing treatment influence the Zn/S atomic ratio, consistent with the controlled incorporation of the elements during CBD and limited sulfur redistribution upon thermal treatment.

Discussion

The structural, optical, morphological, and compositional results obtained in this work can be interpreted coherently within the framework of CBD growth kinetics and quantum confinement physics. Hydrazine hydrate acts simultaneously as a complexing agent that stabilizes Zn^{2+} and as a mild reducing agent that accelerates the formationof free S^{2-} from thiourea. Moderate H.H. concentrations therefore increase nucleation density, leading to smaller crystallites, higher optical band gaps, and improved film compactness, while excessive concentrations promote rapid bulk precipitation and slight agglomeration.

These observations are consistent with the catalytic role of hydrazine reported by Kim et al. and the morphological improvements noted by Lee and Kim [35,41]. The quantum-confinement induced blue-shift of the band gap mirrors trends reported for other nanocrystalline II-VI films near the Bohr radius. Annealing-induced grain growth and the consequent red-shift of the band gap align with numerous prior studies on thermally treated CBD-ZnS.

Photoluminescence spectra confirm the presence of intrinsic vacancies that are only partially annealed out at 300°C, a finding in agreement with earlier luminescence studies of ZnS nanoparticles. The systematic variation of Zn/S stoichiometry with both H.H. concentration and annealing provides an additional degree of freedom for defect engineering that has received limited attention in previous reports.

Table 3 presents a comparative summary of key results from selected published studies and the present work. The present investigation covers a wider and more systematic H.H. concentration range, reports both as-deposited and annealed states for the same sample series, and correlates structural, optical, photoluminescence, morphological, and compositional data. This multi-property, dual state approach highlights the novelty of the work and demonstrates that H.H. concentration is a versatile parameter for tailoring ZnS thin films for Cd-free buffer-layer applications.

Table 3. Comparative summary of selected CBD-ZnS studies employing hydrazine hydrate or related complexants.

H.H. range	Annealing	Properties examined	Key findings	Reference
Limited	Limited	Growth rate, morphology	Enhanced growth for CIGS	[35]
Selected	No	Morphology, growth	Complexant effect	[41]
Review	Various	Multiple variables	Sensitivity to bath chemistry	[43]
0–2.0 M	Yes (300°C)	XRD, optical, PL, SEM, EDAX	Systematic multi-property tuning	This work

Conclusion

Nanocrystalline cubic ZnS thin films with crystallite sizes of 4-5 nm were successfully deposited by CBD using hydrazine hydrate as a complexing agent. Increasing H.H. concentration enhances nucleation density, reduces particle size, increases optical band gap, and improves film uniformity and compactness. Annealing promotes grain growth, reduces band gap, and yields more compact morphology. Photoluminescence confirms near-band-edge emission and defect-related transitions associated with S and Zn vacancies. EDAX reveals systematic changes in Zn/S ratio controlled by H.H. concentration and annealing. These results demonstrate that H.H. concentration is a powerful parameter of nanocrystalline ZnS thin films for opto-electronic devices.

The ability to tune crystallite size, optical band gap, defect density and film stoichiometry simply by adjusting H.H. concentration offers immediate practical value for the fabrication of Cd-free ZnS buffer layers in CIGS and CZTS thin-film solar cells, as well as for electroluminescent devices, sensors and other optoelectronic applications that require wide-band-gap, nanocrystalline semiconductor films. The improved uniformity and compactness achieved at moderate H.H. concentrations (especially ~1.0 M) are particularly advantageous for large-area conformal coatings.

Current limitations of the study include the relatively narrow range of annealing temperatures explored, the absence of precise in-situ thickness monitoring during deposition, and the lack of long-term environmental-stability data. Future work will therefore focus on film-thickness control, extended thermal and humidity stability tests, and direct integration of the optimized ZnS layers into complete photovoltaic devices.

Ethical Statement

No human or animal subjects were involved in this study. All experimental procedures complied with the institutional guidelines of the respective departments.

https://doi.org/10.61577/jnd.2023.100008

Declaration of Competing Interests

The authors declare that they have no known competing financial interests or personal relationships that could have appeared to influence the work reported in this paper.

References

1. Gaponenko SV. Optical Properties of Semiconductor Nanocrystals, Cambridge University Press, Cambridge (1998).
2. Fang X, Zhai T, Gautam UK, Li L, Wu L, Bando Y, et al. ZnS nanostructures: From synthesis to applications. Prog Mater Sci. 2011;56(2):175-287. https://doi.org/10.1016/j.pmatsci.2010.10.001
3. Cullity BD. Elements of X-ray Diffraction. Hsin Yueh; 1986.
4. Zakerian F, Kafashan H. Investigation the effect of annealing parameters on the physical properties of electrodeposited ZnS thin films. Superlattices and Microstruct. 2018;124:92-106. https://doi.org/10.1016/j.spmi.2018.09.039
5. Nakada T, Mizutani M. 18% efficiency Cd-free Cu (In, Ga) Se2 thin-film solar cells fabricated using chemical bath deposition (CBD)-ZnS buffer layers. Jpn J Appl Phys. 2002;41(2B):L165. https://doi.org/10.1143/JJAP.41.L165
6. Barkhouse DA, Gunawan O, Gokmen T, Todorov TK, Mitzi DB. Device characteristics of a 10.1% hydrazine-processed Cu2ZnSn (Se, S) 4 solar cell Prog Photovolt: Res Appl. 2012;20(1):6-11. https://doi.org/10.1002/pip.1160
7. Naghavi N, Abou-Ras D, Allsop N, Barreau N, Bücheler S, Ennaoui A, et al. Buffer layers and transparent conducting oxides for chalcopyrite Cu (In, Ga)(S, Se) 2 based thin film photovoltaics: present status and current developments. Prog Photovolt: Res Appl. 2010;18(6):411-433. https://doi.org/10.1002/pip.955
8. Kulkarni SK. Nanotechnology: Principles and practices. Latest Edition. New Delhi: Springer Cham; 2015. 1-403. https://doi.org/10.1007/978-3-319-09171-6
9. Brus LE. Electron-electron and electron-hole interactions in small semiconductor crystallites: The size dependence of the lowest excited electronic state. J Chem Phys. 1984;80(9):4403-4409. https://doi.org/10.1063/1.447218
10. Efros AL, Rosen M. The electronic structure of semiconductor nanocrystals. Annu Rev Mater Sci. 2000;30(1):475-521. https://doi.org/10.1146/annurev.matsci.30.1.475
11. D'Amore M, Takasao G, Chikuma H, Wada T, Taniike T, Pascale F, et al. Understanding structure and properties of MgCl2 supported Ziegler-Natta Nanoclusters by DFT, spectroscopy and machine learning: How modelling uncovers the origin of industrial catalysis. In1st International Conference on Computational & Applied Physics; 2022; p8. https://doi.org/10.21467/abstracts.122
12. Kassim A, Nagalingam S, Min HS, Karrim N. XRD and AFM studies of ZnS thin films produced by electrodeposition method. Arab J Chem. 2010;3(4):243-249.
13. Kavanagh Y, Alam MJ, Cameron DC. The characteristics of thin film electroluminescent displays produced using sol-gel produced tantalum pentoxide and zinc sulfide. Thin Solid Films. 2004;447:85-89. https://doi.org/10.1016/j.tsf.2003.09.027
14. Zhang H, Deng J, Pan Z, Bai Z, Kong L, Wang J. Structural and optical properties of Nb-doped β-Ga2O3 thin films deposited by RF magnetron sputtering. Vacuum. 2017;146:93-96. https://doi.org/10.1016/j.vacuum.2017.09.033
15. Gayou VL, Salazar-Hernandez B, Constantino ME, Andrés ER, Díaz T, Macuil RD, et al. Structural studies of ZnS thin films grown on GaAs by RF magnetron sputtering. Vacuum. 2010;84(10):1191-1194. https://doi.org/10.1016/j.vacuum.2009.10.023
16. Kim YS, Yun SJ. Studies on polycrystalline ZnS thin films grown by atomic layer deposition for electroluminescent applications. Appl Surf Sci. 2004;229(1-4):105-111. https://doi.org/10.1016/j.apsusc.2004.01.050
17. Lee EY, Tran NH, Lamb RN. Growth of ZnS films by chemical vapor deposition of Zn [S2CN (CH3)2] 2 precursor. Appl Surf Sci. 2005;241(3-4):493-496. https://doi.org/10.1016/j.apsusc.2004.07.003
18. Lee EY, Tran NH, Russell JJ, Lamb RN. Structure evolution in chemical vapor-deposited ZnS films. J Phys Chem B. 2003;107(22):5208-5211. https://doi.org/10.1021/jp027366d
19. Elidrissi B, Addou M, Regragui M, Bougrine A, Kachouane A, Bernede JC. Structure, composition and optical properties of ZnS thin films prepared by spray pyrolysis. Mater Chem Phys. 2001;68(1-3):175-179. https://doi.org/10.1016/S0254-0584(00)00351-5
20. Djelloul A, Adnane M, Larbah Y, Sahraoui T, Zegadi C, Maha A, et al. Properties study of ZnS thin films prepared by spray pyrolysis method. JNano- Electron Phys. 2015;7(4):40405(1-5).
21. Kennedy J, Murmu PP, Gupta PS, Carder DA, Chong SV, Leveneur J, et al. Effects of annealing on the structural and optical properties of zinc sulfide thin films deposited by ion beam sputtering. Mater Sci Semicond Process. 2014;26:561-566. https://doi.org/10.1016/j.mssp.2014.05.055
22. Zhang W, Zeng X, Lu J, Chen H. Phase controlled synthesis and optical properties of ZnS thin films by pulsed laser deposition. Mater Res Bull. 2013;48(10):3843-3846. https://doi.org/10.1016/j.materresbull.2013.05.084
23. Yang K, Li B, Zeng G. Effects of temperature on properties of ZnS thin films deposited by pulsed laser deposition. Superlattices Microstruct. 2019;130:409-415. https://doi.org/10.1016/j.spmi.2019.05.009
24. Roy P, Ota JR, Srivastava SK. Crystalline ZnS thin films by chemical bath deposition method and its characterization. Thin Solid Films. 2006;515(4):1912-1917. https://doi.org/10.1016/j.tsf.2006.07.035
25. Hong J, Lim D, Eo YJ, Choi C. Chemical bath deposited ZnS buffer layer for Cu (In, Ga) Se2 thin film solar cell. Appl Surf Sci. 2018;432:250-254. https://doi.org/10.1016/j.apsusc.2017.09.133
26. Liu WL, Yang CS, Hsieh SH, Chen WJ, Fern CL. Effect of deposition variables on properties of CBD ZnS thin films prepared in chemical bath of ZnSO4/SC (NH2) 2/Na3C3H5O7/NH4OH. Appl Surf Sci. 2013;264:213-218. https://doi.org/10.1016/j.apsusc.2012.09.174
27. Nasr TB, Kamoun N, Kanzari M, Bennaceur R. Effect of pH on the properties of ZnS thin films grown by chemical bath deposition. Thin Solid Films. 2006;500(1-2):4-8. https://doi.org/10.1016/j.tsf.2005.11.030
28. Bayer A, Boyle DS, O'Brien P. In situ kinetic studies of the chemical bath deposition of zinc sulfide from acidic solutions. J Mater Chem. 2002;12(10):2940-2944. https://doi.org/10.1039/b205158n
29. Hodes G. Chemical solution deposition of semiconductor films. CRC press; 2002.
30. Nair PK, Nair MT, Garcıa VM, Arenas´O, Pena Y, Castillo A, et al. Semiconductor thin films by chemical bath deposition for solar energy related applications. Sol Energy Mater Sol Cells. 1998;52(3-4):313-344. https://doi.org/10.1016/S0927-0248(97)00237-7
31. Venables J. Introduction to surface and thin film processes. Cambridge University Press; 2000.
32. Dona JM, Herrero J. Process and film characterization of chemical-bath-deposited ZnS thin films. J Electrochem Soc. 1994;141(1):205-210. https://doi.org/10.1149/1.2054685
33. Oladeji IO, Chow L. Synthesis and processing of CdS/ZnS multilayer films for solar cell application. Thin Solid Films. 2005;474(1-2):77-83. https://doi.org/10.1016/j.tsf.2004.08.114

https://doi.org/10.61577/jnd.2023.100008

34. Goudarzi A, Aval GM, Sahraei R, Ahmadpoor H. Ammonia-free chemical bath deposition of nanocrystalline ZnS thin film buffer layer for solar cells. Thin Solid Films. 2008;516(15):4953-4957. https://doi.org/10.1016/j.tsf.2007.09.051
35. Kim J, Lee CR, Arepalli VK, Kim SJ, Lee WJ, Chung YD. Role of hydrazine in the enhanced growth of zinc sulfide thin films using chemical bath deposition for Cu (In, Ga) Se2 solar cell application. Mater Sci Semicond Process. 2020;105:104729. https://doi.org/10.1016/j.mssp.2019.104729
36. Lekiket H, Aida MS. Chemical bath deposition of nanocrystalline ZnS thin films: Influence of pH on the reaction solution. Mater Sci Semicond Process. 2013;16(6):1753-1758. https://doi.org/10.1016/j.mssp.2013.06.028
37. Kang SR, Shin SW, Choi DS, Moholkar AV, Moon JH, Kim JH. Effect of pH on the characteristics of nanocrystalline ZnS thin films prepared by CBD method in acidic medium. Curr Appl Phys. 2010;10(3):S473-S477. https://doi.org/10.1016/j.cap.2010.02.052
38. Deepa K, Preetha KC, Murali KV, Dhanya AC, Ragina AJ, Remadevi TL. The effect of various complexing agents on the morphology and optoelectronic properties of chemically deposited ZnS thin films: A comparative study. Optik. 2014;125(19):5727-5732. https://doi.org/10.1016/j.ijleo.2014.06.028
39. Liu Q, Mao G. Comparison of CdS and ZnS thin films prepared by chemical bath deposition. Surf Rev Lett. 2009;16(03):469-474. https://doi.org/10.1142/S0218625X09012871
40. Agawane GL, Shin SW, Moholkar AV, Gurav KV, Yun JH, Lee JY, et al. Non-toxic complexing agent Tri-sodium citrate's effect on chemical bath deposited ZnS thin films and its growth mechanism. J Alloys Compd. 2012;535:53-61. https://doi.org/10.1016/j.jallcom.2012.04.073
41. Lee, Cha-ran, & Kim, Je-ha. Hydrazine effect on ZnS thin film growth by the CBD method. J. Korean Inst Electr Electron Mater Eng. 2018;31(3):177-181. https://doi.org/10.4313/JKEM.2018.31.3.177
42. Isi PO, Jeroh DM, Isah J, Obiajulu O, Ndukwe FO. Effect of complexing agent on the optical properties of zinc sulphide (ZnS) thin films using chemical bath deposition. Int Multidiscip Res J Rev. 2025;2(4). https://doi.org/10.17148/IMRJR.2025.020415
43. Arsad AZ, Zuhdi AWM, Abdullah SF, Chau CF, Ghazali A, Ahmad I, et al. Effect of chemical bath deposition variables on the properties of zinc sulfide thin films: A review. Molecules. 2023;28(6):2780. https://doi.org/10.3390/molecules28062780
44. Zhou L, Xue Y, Li J. Study on ZnS thin films prepared by chemical bath deposition. J Environ Sci China. 2009;21:S76-S79. https://doi.org/10.1016/S1001-0742(09)60042-5
45. Joint Committee on Powder Diffraction Standards (JCPDS) Card No. 05-0566 (cubic ZnS).
46. Maissel LI, Glang R. Handbook of thin film technology.
47. Scherrer PJ. Nachr Ges wiss goettingen. Math Phys. 1918;2:98-100.
48. Antony A, Murali KV, Manoj R, Jayaraj MK. The effect of the pH value on the growth and properties of chemical-bath-deposited ZnS thin films. Mater Chem Phys. 2005;90(1):106-110. https://doi.org/10.1016/j.matchemphys.2004.10.017
49. Lokhande CD, Patil PS, Tributsch H, Ennaoui A. ZnSe thin films by chemical bath deposition method. Sol Energy Mater Sol Cells. 1998;55(4):379-393. https://doi.org/10.1016/S0927-0248(98)00112-3
50. Meshram RS, Thombre RM. Structural and optical properties of ZnS thin films deposited by spray pyrolysis technique. 2011;14(2).
51. Sahraei R, Aval GM, Goudarzi A. Compositional, structural, and optical study of nanocrystalline ZnS thin films prepared by a new chemical bath deposition route. J Alloys Compd. 2008;466(1-2):488-492. https://doi.org/10.1016/j.jallcom.2007.11.127
52. Kumbhojkar N, Nikesh VV, Kshirsagar A, Mahamuni S. Photophysical properties of ZnS nanoclusters. J Appl Phys. 2000;88(11):6260-6264. https://doi.org/10.1063/1.1321027
53. Becker WG, Bard AJ. Photoluminescence and photoinduced oxygen adsorption of colloidal zinc sulfide dispersions. J Phys Chem. 1983;87(24):4888-4893. https://doi.org/10.1021/j150642a026
54. Denzler D, Olschewski M, Sattler K. Luminescence studies of ZnS nanoparticles. J Appl Phys. 1998;84(5):2841-2845. https://doi.org/10.1063/1.368425
55. Gumus C. Effects of annealing on optical properties of ZnS and ZnS: Mn thin films. J Optoelectron Adv Mater. 2010;12(8):1747-1751.
56. Márquez E, Shaaban ER, Abousehly AM. Structural and optical properties of ZnS thin films. Int J New Hor Phys. 2014;1(1):17-24.
57. Liu J, Wei A, Zhao Y. Effect of different complexing agents on the properties of chemical-bath-deposited ZnS thin films. J Alloys Compd. 2014;588:228-234.
58. Sartale SD, Sankapal BR, Lux-Steiner M, Ennaoui A. Preparation of nanocrystalline ZnS by a new chemical bath deposition route. Thin Solid Films. 2005;480:168-172. https://doi.org/10.1016/j.tsf.2004.11.054

https://doi.org/10.61577/jnd.2023.100008